J Solid State Electrochem (2012) 16:1693–1700
DOI 10.1007/s10008-011-1576-4

ORIGINAL PAPER

A novel hydrogen peroxide sensor based on Ag nanoparticles electrodeposited on chitosan-graphene oxide/cysteamine-modified gold electrode

Li Wang · Haozhi Zhu · Haoqing Hou · Zhiyao Zhang · Xianping Xiao · Yonghai Song

Received: 30 June 2011 / Revised: 6 October 2011 / Accepted: 16 October 2011 / Published online: 13 November 2011

Abstract A novel strategy to fabricate a hydrogen peroxide sensor based on Ag nanoparticles electrodeposited on chitosan-graphene oxide nanocomposites/cysteamine-modified gold (Au) electrode was reported. The chitosan-graphene oxide nanocomposites were first assembled on a cysteamine-modified Au electrode to produce chitosan-graphene oxide/cysteamine/Au electrode. Then Ag nanoparticles were electrodeposited on the modified Au electrode and formed Ag nanoparticles/chitosan-graphene oxide/cysteamine/Au electrode. The chitosan-graphene oxide nanocomposites and the electrodeposited Ag nanoparticles were characterized by atomic force microscopy and scanning electron microscopy. The results showed the Ag nanoparticles were uniformly dispersed on the chitosan-graphene oxide/cysteamine/Au electrode. The cyclic voltammagrams and amperometric method were used to evaluate electrocatalytic properties of the Ag nanoparticles/chitosan-graphene oxide/cysteamine/Au electrode. The results showed that the modified electrode displayed good electrocatalytic activity to the reduction of hydrogen peroxide with a detection limit of 0.7 μM hydrogen peroxide based on a signal-to-noise ratio of 3. The sensor has good reproducibility, wide linear range, and long-term stability.

Keywords Sensor · Graphene oxide · Chitosan · Electrodeposition · Ag nanoparticles

L. Wang (✉) · H. Zhu · H. Hou · Z. Zhang · X. Xiao · Y. Song
College of Chemistry and Chemical Engineering,
Jiangxi Normal University,
99 Ziyang Road,
Nanchang 330022, People's Republic of China
e-mail: lwang@jxnu.edu.cn

Y. Song
e-mail: yhsong@jxnu.edu.cn

Introduction

The accurate determination of hydrogen peroxide (H_2O_2) has become extremely important in recent years because H_2O_2 is widely used in food, pharmaceutical, chemical and biochemical industries. Many methods such as titrimetry [1], spectrofluorometry [2, 3], spectrophotometry [4, 5], chemiluminescence [6], and electrochemistry [7, 8] have been used to detect H_2O_2.

Recently, electrochemical method has attracted much attention due to its low cost and high sensitivity. Mediating metal or metal oxide nanoparticles (NPs) on an electrode as a catalyst, which can determine the amount of trace H_2O_2 exactly, is a hot topic owing to their large specific surface areas, excellent conductivities, and catalytic activities. Many NPs, including gold (Au) NPs [9–11], Ag NPs [12], Pd NPs [13], Pt NPs [14–16], SiO_2 NPs [17], etc., have been widely used to construct electrochemical sensors for H_2O_2 detection. Among these sensors, the sensor based on Ag NPs exhibited an extremely fast amperometric response, a low detection limit and a wide linear range to detect H_2O_2. A large number of studies showed the sensor's property depended strongly on the size, distribution and shape of Ag NPs on electrode [18–20].

To obtain a good catalytic activity, electrodeposition of Ag^+ in a solution containing DNA molecules or chitosan (CHIT) molecules to produce small Ag NPs by decreasing the reduction rate of Ag^+ have been developed [21]. However, the size of produced Ag NPs was about 100 nm, and the packed density of Ag NPs was very high, which were unfavorable for catalytic activity due to the decrease of catalytic sites. DNA and collagen assembled on electrode surface resulted in the formation of small Ag NPs owing to their porous networks and accordingly improved catalytic activity of the resulted sensor [18, 19]. Some

conductive materials, such as carbon nanotubes [22], supramolecular microfibrils of *o*-phenylenediamine [23], and carbon nanofibers [24], have also been used to modify electrode for Ag NPs deposition as sensor for H_2O_2 detection. Graphene, a single layer of carbon atoms in a closely packed honeycomb two-dimensional lattice, has attracted tremendous attention because of its excellent electrical properties and the high specific surface area of 400 m^2/g up to 1,500 m^2/g for metal NPs deposition or enzyme adsorption on electrodes [25–29], especially graphene oxide (GO) or chemically derived graphene owing to its abundant groups, such as epoxide, hydroxyl and carboxylic groups, and the high water solubility [30–36]. The remarkable surface area and its well electrocatalytic and electrochemical properties have led to an explosion of research in the field of electrochemical sensors.

In this work, Ag NPs were electrodeposited on CHIT-GO nanocomposites that were firstly assembled on cysteamine/Au electrode to fabricate a H_2O_2 sensor. The CHIT has been widely used as a matrix to immobilize enzyme or NPs due to its abundant groups. The CHIT-GO nanocomposites resulted in the formation and uniform dispersion of small Ag NPs in sequent Ag^+ electrodepositing. The produced Ag NPs exhibited remarkable catalytic activity for H_2O_2 reduction. The analytical performance of the sensor related to the sensitivity, detection limit, linear range, response time, selectivity and stability have been discussed in detail.

Experimental section

Chemicals

Chitosan (CHIT, 75% deacetylation) and cysteamine were purchased from Sigma-Aldrich (St. Louis, USA); 30% H_2O_2 and other reagents were purchased from Beijing Chemical Reagent Factory (Beijing, China) and were of analytical reagent grade. A series of phosphate-buffered solution (PBS; 0.2 M) were used as supporting electrolyte prepared by mixing solution of 0.2 M Na_2HPO_4 and 0.2 M NaH_2PO_4. The solutions were deoxygenated by nitrogen before experiments. All solutions were prepared with ultra-pure water, purified by a Millipore-Q System (18.2 MΩ cm).

Synthesis of CHIT-GO nanocomposites

GO was synthesized according to previous methods [37]. Briefly, graphite powder (1.0 g) was dispersed into 23-mL concentrated H_2SO_4 (18.0 M) in ice bath. Then, $KMnO_4$ (3.0 g) was gradually added into above solution under continuous vigorous stirring at the temperature below 20 °C. After that, the ice bath was replaced by an oil bath and the mixture was heated to 35 °C for 30 min under continuous stirring. Then, ultra-pure water was slowly added into above solution, which produced a rapid increase in solution temperature up to a maximum of 100 °C. The reaction was maintained at 98 °C for a further 15 min, and terminated by sequential addition of more distilled water (140 mL in total) and H_2O_2 (30%, 10 mL). The solid product was separated by centrifugation at 5,000 rpm and washed initially with 5% HCl until SO_4^{2-} ions were no longer detectable with $BaCl_2$. Finally, the solid product was washed three times with acetone and dried overnight at 65 °C.

CHIT-GO nanocomposites were prepared as followed [38]. GO was dissolved in 20 mL of ultra-pure water and treated with ultrasound for 45 min. CHIT solution of 1.0 wt. % was prepared by dissolving CHIT in 0.5 vol.% aqueous acetic acid solution. Then GO solution was added into the CHIT solution and stirred for 24 h to produce a homogeneous CHIT-GO solution.

Electrode modification procedure

The polished Au electrode with surface area of 0.785 mm^2 was immersed in 1.0 mM ethanol solution of cysteamine for 24 h and followed by ultrasonicating thoroughly with ethanol to eliminate physically adsorbed cysteamine. The cysteamine-modified Au electrode was immersed in CHIT-GO solution for 12 h to produce the CHIT-GO/cysteamine/Au electrode. The CHIT-GO/cysteamine/Au electrode was scanned in the potential range from −0.4 to 0.6 V at 50 mV/s for 50 cycles in 0.1 M KNO_3 solution containing 3.0 mM $AgNO_3$ and produced the Ag NPs/CHIT-GO/cysteamine/Au electrode. The procedure for the modified electrode construction was shown in Fig. 1. The modified electrode was stored at 4 °C in a refrigerator when not in use. For comparison, Ag NPs/Au electrode and Ag NPs/cysteamine/Au electrode were also prepared with the same procedure as described above.

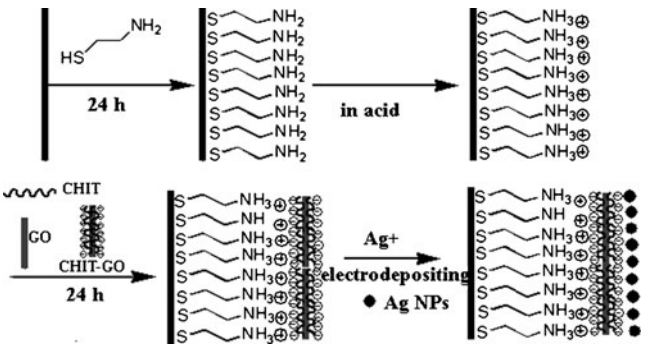

Fig. 1 Schematic representation of the procedure for the electrode construction

Apparatus

All electrochemical experiments were performed by a CHI 660C electrochemical workstation (CH Instruments, Shanghai, China) using a conventional three-electrode system with a platinum wire as the auxiliary electrode, a bare or modified Au electrode as the working electrode, and a saturated calomel electrode (SCE) as the reference electrode. The cyclic

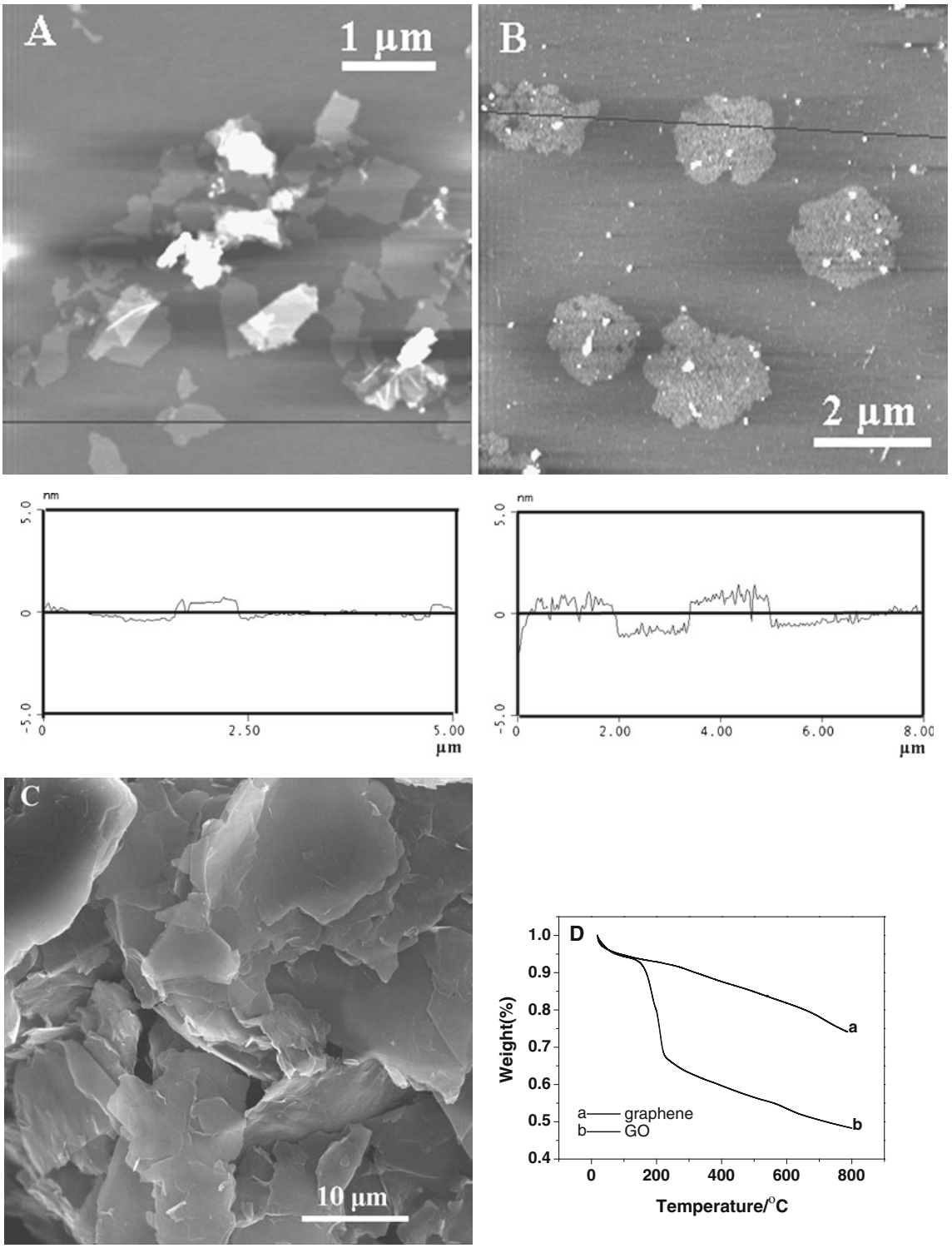

Fig. 2 AFM images of GO (**A**) and CHIT-GO nanocomposites (**B**), and the corresponding to height profile of the AFM images. **C** SEM images of GO. **D** TGA of graphene (**a**) and GO (**b**)

voltammetric experiments were performed in a quiescent solution. The amperometric experiments were carried out in a continuous stirring solution using a magnetic stirrer.

Atomic force microscopy (AFM) measurements were carried out with an AJ-III (Shanghai Aijian Nanotechnology) in tapping mode. Standard silicon cantilevers (spring constant, 0.6–6 N/m) were used under its resonance frequency (typically, 60–150 kHz). The samples for AFM measurement were prepared by dropping the aqueous suspension of GO and CHIT-GO composites on a freshly cleaved mica surface. The scanning electron microscopy (SEM) analysis was taken using a XL30 ESEM-FEG SEM at an accelerating voltage of 20 kV equipped with a Phoenix energy dispersive X-ray analyzer. Thermogravimetric analysis (TGA) was carried out on an SDT 2960 Simultaneous DSC-TGA, TA Instrument.

Results and discussion

Characterization of the sensor construction

The morphology of as-prepared GO and CHIT-GO nanocomposites were characterized by using AFM (Fig. 2A, B) and SEM (Fig. 2C), respectively. GO can be dispersed very well in water at the level of individual sheets because of abundant oxygen-containing functional groups on its surfaces and electrostatic repulsion between the negative charge of GO sheets. Thus, individual sheets could be easily observed on mica surface as shown by AFM image (Fig. 2A) and SEM image (Fig. 2C). The GO has lateral dimensions from several to hundred micrometers (Fig. 2C) with a thickness of 1.0 nm as shown by its section analysis (Fig. 2A), which is characteristic of fully exfoliated GO sheets [38]. The oxygen content of the prepared GO was measured by TGA (Fig. 2D). As shown by curve b in Fig. 2D, there is a sharp decrease at about 200 °C as compared with that of graphene (curve a), which was ascribed to the decomposition of oxygen-containing groups of GO. According to the TGA of GO (curve b), the oxygen content of GO was estimated to be about 41%, which is similar to the previous result [39]. The AFM image of CHIT-GO nanocomposites obviously showed a very rough surface (Fig. 2B), suggesting CHIT and GO formed CHIT-GO nanocomposites based on the strong electrostatic attraction and hydrogen bonding between amino group of CHIT and carboxyl group of GO. The thickness of CHIT-GO sheet was measured by section-analysis to be about 2.0 nm (Fig. 2B). Since the size of the CHIT was about 0.5 nm [38] and the thickness of the GO was about 1 nm, it was reasonable to conclude that the CHIT-GO nanocomposites consisted of one layer of GO and mono- or submonolayer of CHIT on both of its surfaces.

The morphology of the resulted electrode was also characterized by SEM. Fig. 3 showed typical SEM images of Ag NPs/CHIT-GO/cysteamine/Au electrode. A large CHIT-GO sheet was clearly observed and there were lots of small filaments on the sheet (Fig. 3A). The high-magnification SEM image showed that the small filaments were composed of the electrodeposited Ag NPs (Fig 3B). The Ag NPs were firmly embedded in the CHIT-GO matrix and hardly detached from the composite, since no Ag NPs were observed out of the matrix sheets. The average size of the Ag NPs was about 50 nm. These small Ag NPs provided large accessible surface area for the subsequent electrocatalytic reaction of analytes.

Electrochemical behaviors of Ag NPs/CHIT-GO/cysteamine/Au electrode

Figure 4A showed cyclic voltammograms (CVs) of Ag NPs/Au (curve a), Ag NPs/cysteamine/Au (curve b) and Ag NPs/CHIT-GO/cysteamine/Au (curve c) electrode in N_2-saturated 0.2 M PBS solution (pH 7.0). Each CVs showed a

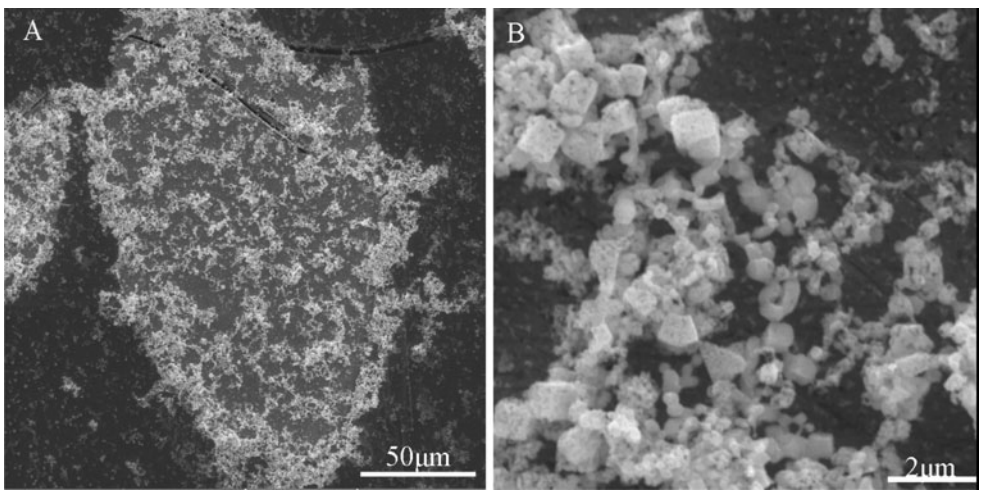

Fig. 3 SEM images of Ag NPs electrodeposited on CHIT-GO/cysteamine/Au substrate: low (**A**) and high (**B**) magnification

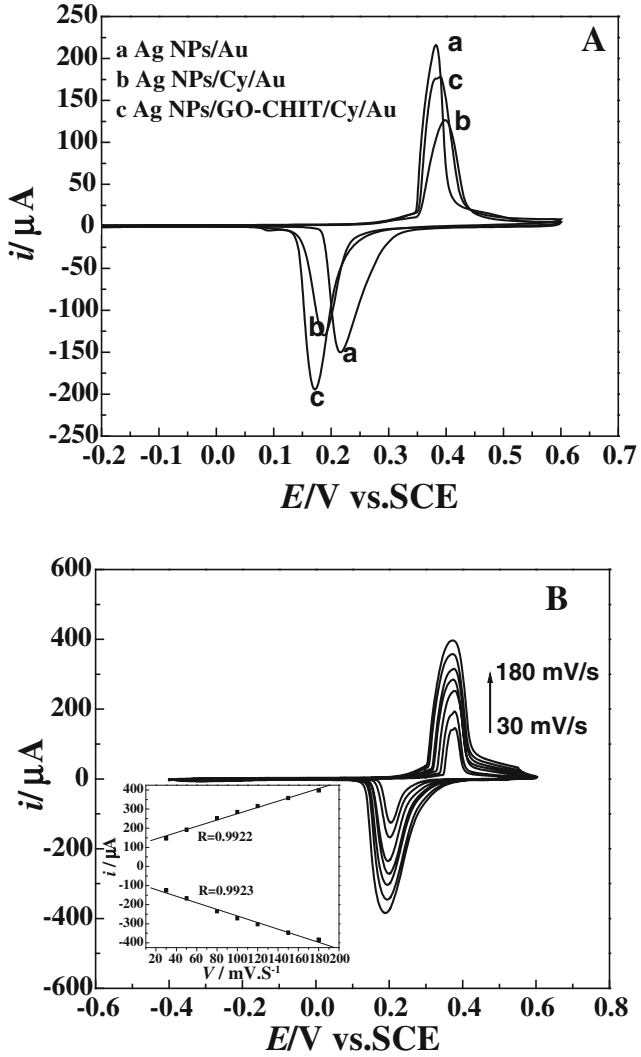

Fig. 4 **A** CVs of Ag NPs/Au (*a*), Ag NPs/cysteamine/Au (*b*) and Ag NPs/CHIT-GO/cysteamine/Au (*c*) electrode in 0.2 M PBS solution (pH 7.0) at a scan rate of 50 mV/s. **B** CVs of Ag NPs/CHIT-GO/cysteamine/Au in 0.2 M PBS solution (pH 7.0) at different scan rates: 30, 50, 80 100, 120, 150, and 180 mV/s, respectively. *Inset*, plot of peak current (i_p) versus scan rate

couple of waves which was ascribed to oxidation of Ag and reduction of Ag^+, respectively. The cathodic peak current of Ag NPs/CHIT-GO/cysteamine/Au electrode (curve c) was obviously larger than that of the other two electrodes (curve a and b), suggesting a large number of Ag NPs produced on Ag NPs/CHIT-GO/cysteamine/Au modified electrode. The anode peak current was smaller than that of Ag NPs/Au (curve a) and larger than that of Ag NPs/cysteamine/Au (curve b), indicating the GO might enhance the electron transfer due to its good conductivity.

The CVs of Ag NPs/CHIT-GO/cysteamine/Au electrode were also recorded at various scan rates ranging from 30 to 180 mV/s in 0.2 M PBS solution (pH 7.0) as shown in Fig. 4B. Obviously, the peak currents were enhanced with the increasing of the scan rate. The peak current is proportional to the scan rate (the inset in Fig. 4B), indicating that the electron-transfer reaction involved with a surface-confined process.

Electrocatalysis of H_2O_2 at the Ag NPs/CHIT-GO/cysteamine/Au electrode

The sensing application of Ag NPs/CHIT-GO/cysteamine/Au electrode was investigated. Fig. 5 showed the CVs of various electrodes in 0.2 M PBS of pH 7.0 in the presence (curve b, c, d, e, f and g) and absence (curve a) of 1.0 mM H_2O_2. In the presence of H_2O_2, an obvious reduction peak appeared at about −0.40 V at the Ag NPs/CHIT-GO/cysteamine/Au electrode (curve g) as compared with that in absence of H_2O_2 (curve a). No obvious peak current was observed at the bare Au electrode (curve b), the cysteamine/Au electrode (curve c) and the CHIT-GO/cysteamine/Au electrode (curve d), which indicated that the current might mainly result from reduction of H_2O_2 catalyzed by Ag NPs. There were also obvious currents at the Ag NPs/cysteamine/Au electrode (curve f) and Ag NPs/Au electrode (curve e), but the current was obviously smaller than that of Ag NPs/CHIT-GO/cysteamine/Au electrode (curve g), indicating the CHIT-GO played a crucial role in the performance of the sensor. Factly, the CHIT-GO nanocomposites provided a large surface area to produce a large number of Ag NPs and accordingly resulted in a large catalytic current. It was noticeable that the peak potential at the Ag NPs/CHIT-GO/cysteamine/Au

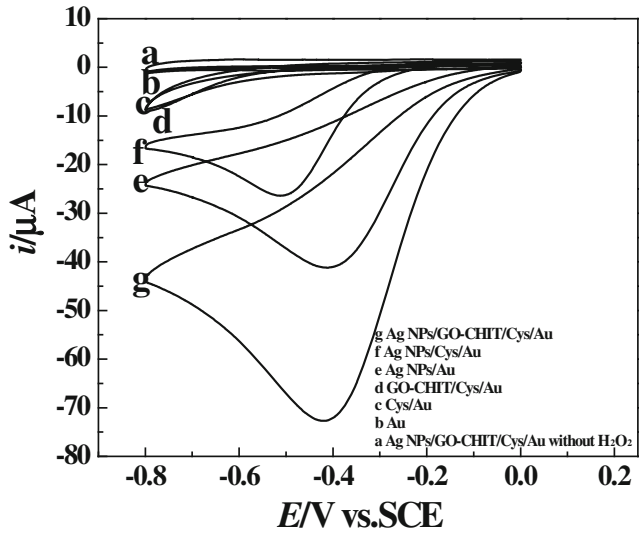

Fig. 5 CVs of various electrodes in 0.2 M PBS (pH 7.0) in the presence (*b*–*g*) and absence (*a*) of 1.0 mM H_2O_2: bare Au electrode (*b*), cysteamine/Au electrode (*c*), CHIT-GO/cysteamine/Au electrode (*d*), Ag NPs/Au electrode (*e*), Ag NPs/cysteamine/Au electrode (*f*), and Ag NPs/CHIT-GO/cysteamine/Au electrode (*a*, *g*). Scan rate, 50 mV/s

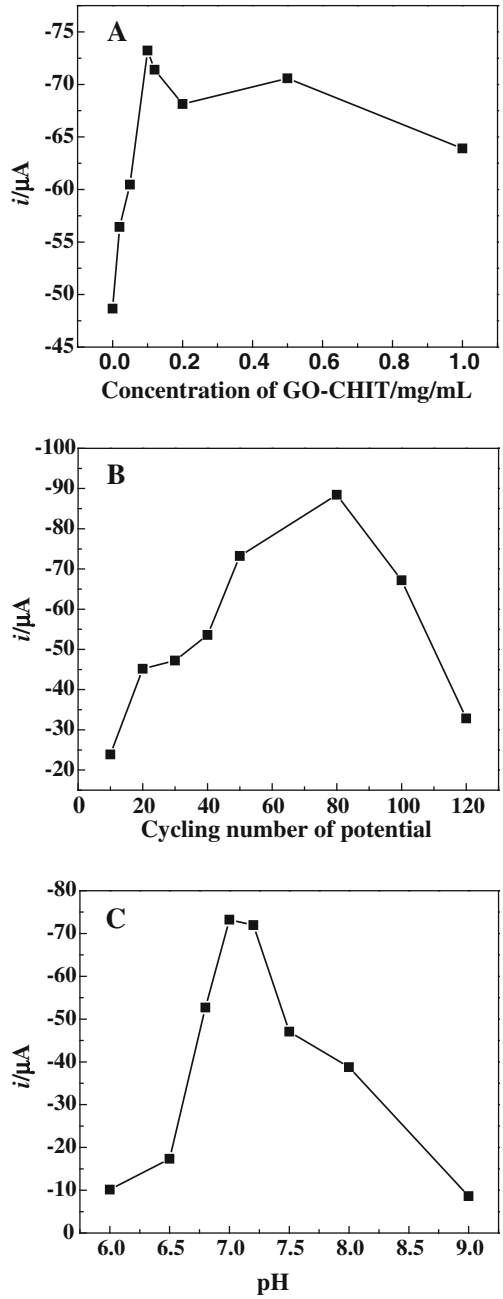

Fig. 6 Effects of concentration of CHIT-GO (**A**), cycling number of potential in the formation process of Ag NPs (**B**), and pH of electrolyte solution (**C**) on the amperometric response in the presence of 1.0 mM H_2O_2 and 0.2 M PBS

electrode was at −0.41 V, which was more positive than that at Ag NPs/cysteamine/Au electrode (−0.53 V) and was similar to that at Ag NPs/Au electrode (−0.41 V). The positive reduction peak potential indicated a fast electron-transfer rate and good electrocatalytic activity toward the reduction of H_2O_2 at the Ag NPs/CHIT-GO/cysteamine/Au electrode.

To optimize the electrocatalytic performance of Ag NPs/CHIT-GO/cysteamine/Au electrode in 0.2 M PBS for reduction of H_2O_2, some factors related to the formation of sensor construction, such as the concentration of CHIT-GO nanocomposites, numbers of potential cycling for formation of Ag NPs and pH of electrolyte solution, were investigated.

The effect of CHIT-GO concentration used for sensor construction on the electrocatalytic reduction of H_2O_2 was investigated and the result was shown in Fig. 6A. There was a noticeable increasing in the current response with the increase of CHIT-GO concentration and the catalytic current reached the maximal value at 0.1 mg/mL. After that, the current decreased gradually as the CHIT-GO concentration further increased. This phenomenon might be ascribed to the following two factors. The lower concentrations resulted in fewer CHIT-GO assembled on electrode surface and accordingly a few Ag NPs was deposited on the CHIT-GO/Au electrode. On the other

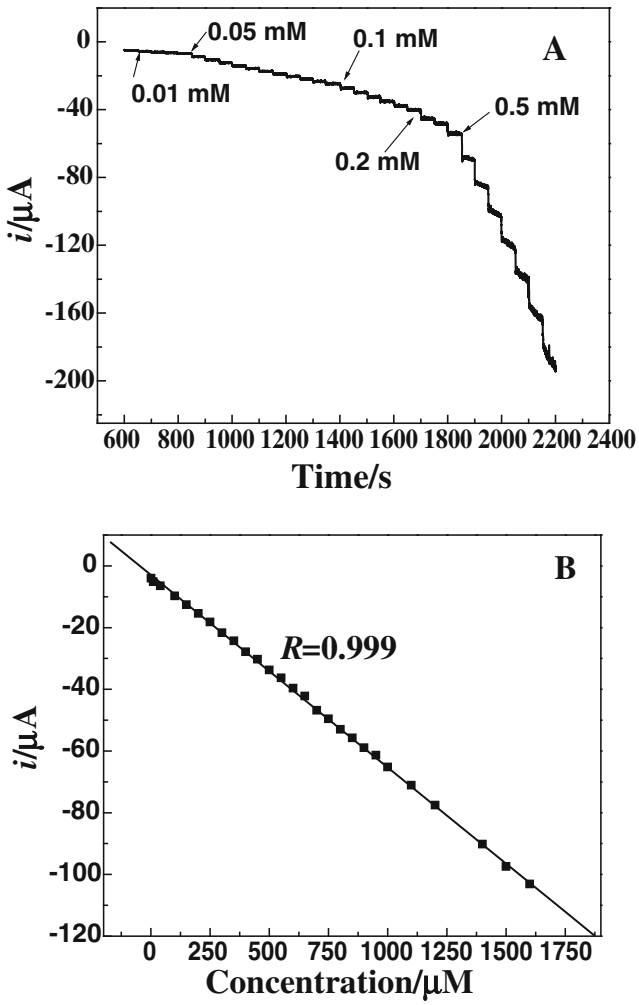

Fig. 7 **A** Typical steady-state response of the Ag NPs/CHIT-GO/cysteamine/Au electrode to successive injection of H_2O_2 into the stirring PBS. **B** The plot of the calibration curve. Applied potential, −0.400 V and supporting electrolyte, 0.2 M PBS of pH 7.0

Table 1 Comparison of the performance of various H_2O_2 sensors constructed from Ag NPs

	Detection limit (μM)	Linear range (mM)	Sensitivity (μA/μM)	References
Ag NPs/GO-CHIT/cysteamine/Au electrode	0.7	0.006–18	0.0624	This work
Ag NPs/PoPD/GCE	1.5	0.006–67.3	0.357	[23]
Ag NPs/DNA/GCE	1.7	0.004.0–16.0	–	[18]
AgNPs/Collagen/GCE	0.7	0.005–40.6	–	[19]
Ag NPs-NFs/GCE	62	0.10–80.0	–	[22]
Ag NPs-GN-R/GCE	28	0.1–40.0	–	[24]
Ag NPs-MWCNT/Au electrode	0.5	0.05–17	1.42×10^{-3}	[40]

NPs nanoparticles, *GO* graphene oxide, *CHIT* chitosan, *GCE* glassy carbon electrode *CNT* carbon nanotube

hand, the higher CHIT-GO concentration might lead to compact CHIT-GO film on the electrode surface. The compact CHIT-GO film would produce some Ag blocks and accordingly decreased the effective area of Ag catalyst on electrode surface. Thus, the optimal concentration of CHIT-GO for sensor construction was 0.1 mg/mL.

Figure 6B showed the effect of number of potential cycling in the formation process of Ag NPs on the reduction of H_2O_2. The number of potential cycling would control the amount and size of the Ag NPs on electrode surface. A few Ag NPs was deposited on the electrode at the less number of potential cycling, which would result in a poor catalytic activity. With the number of potential cycling increasing, more and more Ag NPs were formed. As shown in Fig. 6B, the maximal value appeared at 80 cycles. This turning point might be ascribed to the fact that the Ag NPs would become rather bigger with the excessive number of potential cycling, which could decrease its electrocatalytic ability.

The effect of the pH of the buffer solution on the catalytic reduction of H_2O_2 was also investigated. Fig. 6C showed the plot of amperometric responses of the sensor versus different pH in 0.2 M PBS (6.0–9.0) in the presence of 1.0 mM H_2O_2. The Ag NPs/CHIT-GO/cysteamine/Au electrode showed best electrocatalytic activity in buffer solution of pH 7.0.

Figure 7A showed the typical steady-state current response of the sensor on successive addition of H_2O_2 into stirring 0.2 M PBS (pH 7.0). When H_2O_2 was added, the reduction current rose sharply to reach a maximum steady-state value and achieved 95% of steady-state current within 2 s. The fast response was mainly ascribed to the fact that the CHIT-GO nanocomposites greatly enlarged the total surface area of the Ag NPs and enhanced the electron transfer. Figure 7B showed the corresponding calibration curves for H_2O_2. The response of Ag NPs/CHIT-GO/cysteamine/Au electrode was linear within H_2O_2 concentration from 6.0 μM−18.0 mM (R=0.999, n=20). The detection limit was estimated to be 0.7 μM based on a signal-to-noise ratio of 3. A comparison of the performance of our newly designed sensor with those already reported in literature work regarding the performance of the H_2O_2 assay is shown in Table 1. Up to now, many sensors have been developed based on Ag NPs for the detection of H_2O_2, and all of them have some advantages and limitations [18, 19, 33, 34]. Taking Ag NPs/collagen/GCE [19] as an example, the detection limit was pretty low. While, the linear range was rather small. Recently, Ag NPs decorated graphene modified SCE were constructed for the detection of H_2O_2 with a detection limit of 28 μM and a linear range of 0.1 to 40 mM [34]. Compared with those sensors, the linear response range, the sensitivity and detection limit for H_2O_2 detection of the sensor prepared in this work were much better than some other results.

Selectivity, stability, and reproducibility

Interference is inevitable in the determination of some analyses. Some interference was also investigated in our work. Chemicals such as BrO_3^-, SO_4^{2-}, and SO_3^{2-} in a 2-fold concentration did not show interference to H_2O_2 detection, while IO_3^- and Fe^{3+} in 2-fold concentration interfered significantly H_2O_2 detection. The results were summarized in Table 2.

The stability of the sensor was also investigated in our work. After the sensor was stored in the inverted beaker at 4 °C for 30 days, the current response to 1.0 mM H_2O_2 decreased only 1.2% of the original current. The reproducibility of the current signal for the same electrode to 1.0 mM H_2O_2 was examined in 0.2 M PBS (pH 7.0). The relative standard deviation (RSD) was 4.6% for six

Table 2 Effects of interferences on the catalytic current of the Ag NPs/CHIT-GO/cysteamine/Au electrode

Interferences substrates (mM)							
Responding substrate	IO_3^-	BrO_3^-	SO_4^{2-}		SO_3^{2-}		Fe^{3+}
	Saturated	Saturated	2	5	2	5	2
H_2O_2	_[a]	_[b]	_[b]	_[b]	_[b]	_[b]	_[a]

[a] Interference (variance of catalytic current, >6%)

[b] No interference (variance of catalytic current, ≤6%)

successive measurements. The electrode-to-electrode reproducibility was determined in the presence of 1.0 mM H_2O_2 in 0.2 M PBS (pH 7.0) with seven different electrodes, which yielded a RSD of 4.2%.

Conclusions

In summary, a novel strategy had been introduced to fabricate H_2O_2 sensor based on Ag NPs electrodeposited on the CHIT-GO nanocomposites modified cysteamine/Au electrode. Our experiments confirmed that when the CHIT-GO concentration was 0.1 mg/mL, the numbers of potential cycling was 80 and pH of PBS was 7.0, the sensor showed the maximal electrocatalytic ability for the reduction of H_2O_2. The resulted sensor exhibited fast amperometric response, low detection limit and wide linear range to H_2O_2 detection. Moreover, it also had high sensitivity, good reproducibility and stability. These good properties might mainly benefit from the large surface area and the high quality of the sp^2-conjugated bond in the carbon lattice of GO. Thus, it is considered to be an ideal candidate for practical application.

Acknowledgments This work was financially supported by National Natural Science Foundation of China (20874041, 20905032, 21065005, 21174058), Natural Science Foundation of Jiangxi Province (2008GZH0028), Foundation of Jiangxi Educational Committee (GJJ10389), the State Key Laboratory of Electroanalytical Chemistry (2008003), and the Scientific Research Foundation for the Returned Overseas Chinese Scholars, State Education Ministry.

References

1. Hurdis EC, Romeyn H Jr (1954) Anal Chem 269:320–325
2. Manzoori J, Amjadi M, Orooji M (2006) Anal Sci 22:1201–1206
3. Tang B, Zhang L, Xu K (2006) Talanta 68:876–882
4. Wei H, Wang EK (2008) Anal Chem 80:2250–2254
5. Chang Q, Deng K, Zhu L, Jiang G, Yu C, Tang H (2009) Microchim Acta 165:299–305
6. Li X, Zhou Y, Zheng Z, Yue X, Dai Z, Liu S, Tang Z (2009) Langmuir 25:6580–6586
7. Wang J (2008) Chem Rev 108:814–825
8. Bahshi L, Frasconi M, Tel-Vered R, Yehezkeli O, Willner I (2008) Anal Chem 20:8253–8259
9. Qiu JD, Peng HZ, Liang RP, Li J, Xia XH (2007) Langmuir 23:2133–2137
10. Cui H, Wang W, Duan CF, Dong YP, Guo JZ (2007) Chem Eur J 13:6975–6984
11. Kumar SA, Wang S, Chang YT (2010) Thin Solid Films 518:5832–5838
12. Bui MPN, Pham XH, Han KN, Li CA, Kim YS, Seong GH (2010) Sensor Actuat B-Chem 150:436–437
13. Tang YH, Cao Y, Wang SP, Shen GL, Yu RQ (2006) Sensor Actuat B-Chem 137:736–740
14. Chakraborty S, Retna RC (2009) Biosens Bioelectron 24:3264–3268
15. Niazov T, Shlyahovsky B, Willner L (2007) J Am Chem Soc 129:6374–6375
16. Kicela A, Daniele S (2006) Talanta 68:1632–1639
17. Sun YY, Yan F, Yang WS, Sun CQ (2006) Biomaterials 27:4042–4053
18. Cui K, Song YH, Yao Y, Huang ZZ, Wang L (2008) Electrochem Commun 10:663–667
19. Song YH, Cui K, Wang L (2009) Nanotechnology 20:105501–105508
20. Riskin M, Tel-Vered R, Willner I (2009) Adv Funct Mater 19:2474–2480
21. Wu S, Zhao H, Ju H, Shi C, Zhao J (2006) Electrochem Commun 8:1197–203
22. Shie JW, Yogeswaran U, Chen MS (2010) Talanta 78:896–902
23. Tian JQ, Liu S, Sun XP (2010) Langmuir 26:15112–15116
24. Gajendran P, Saraswathi R (2007) J Phys Chem C 111:11320
25. Liu L, Ryu S, Tomasik MR, Stolyarova E, Jung N, Hybertsen MS, Steigerwald ML, Brus LE, Flynn GW (2008) Nano Lett 8:1965–1970
26. Calizo I, Balandin AA, Bao W, Miao F, Lau CN (2007) Nano Lett 7:2645–2649
27. Geim AK, Novoselov KS (2007) Nature 446:183–191
28. Meyer JC, Geim AK, Katsnelson MI, Novoselov KS, Booth TJ, Roth S (2007) Nature 446:60–63
29. Ishigami M, Chen JH, Cullen WG, Fuhrer MS, Williams ED (2007) Nano Lett 7:1643–1668
30. Fang Y, Guo S, Zhu C, Zhai Y, Wang E (2010) Langmuir 26:11277–11282
31. Shan C, Yang H, Han D, Zhang Q, Ivaska A, Niu L (2010) Biosens Bioelectron 25:1070–1074
32. Zhou M, Zhai Y, Dong S (2009) Anal Chem 81:5603–5613
33. Shan C, Yang H, Song J, Han D, Ivaska A, Niu L (2009) Anal Chem 81:2378–2382
34. Dey RS, Raj CR (2010) J Phys Chem C 114:21427–21433
35. Hong W, Bai H, Xu Y, Yao Z, Gu Z, Shi G (2010) J Phys Chem C 114:1822–1826
36. Cao L, Liu Y, Zhang B, Lu L (2010) ACS Appl Mater Interf 2:2339–2346
37. Hummers W, Offeman R (1958) J Am Chem Soc 80:1339
38. Han D, Han T, Shan C, Ivaska A, Niu L (2010) Electroanal 22:2001–2008
39. Gao W, Alemany LB, Ci L, Ajayan P (2010) m. Nature Chem 1:403–408
40. Zhao W, Wang HQ, Wang X, Zhao Z, Miao Z, Chen L, Shan M, Fang QY (2009) Talanta 80:1029–1033